Biophysical Journal, Volume 97

Supporting Material

Microfilament orientation constrains vesicle flow and spatial distribution in growing pollen tubes.

Jens Helmut Kroeger, Firas Bou Daher, Martin Grant, and Anja Geitmann

Supporting material for *Microfilament orientation constrains vesicle flow and spatial distribution in growing pollen tubes.*

Jens H. Kroeger[1]
Ernest Rutherford Physics Building, McGill University.
Montréal, Québec. Canada H3A 2T8

Firas Bou Daher
Institut de recherche en biologie végétale,
Département de sciences biologiques,
Université de Montréal. Montréal, Québec. Canada H1X 2B2

Martin Grant
Ernest Rutherford Physics Building, McGill University.
Montréal, Québec. Canada H3A 2T8

Anja Geitmann
Institut de recherche en biologie végétale,
Département de sciences biologiques,
Université de Montréal. Montréal, Québec. Canada H1X 2B2

[1]Corresponding author. Address: Ernest Rutherford Physics Building, McGill University. 3600 rue University, Montréal, Québec. Canada. H3A 2T8. Tel.: (514)398-7025, Fax: (524)398-8434

Cell wall expansion

Pollen tube elongation is due to stress induced expansion of its cell wall. Although the physical relations between stress σ and viscoplastic deformation rate $\dot{\epsilon}$ are firmly established, the precise role of the turgor pressure in the growth regulation remains ill defined. Decreasing the turgor below a critical level stops growth (1) and modulating the osmolarity induces variations in the tube growth rate (2, 3). While expansion rate and stress variations can be caused by many different factors such as cell wall thickness, extensibility and turgor, the viscoplastic expansion rate and stress in the plant cell wall generally obey Lockhart's equation $\dot{\epsilon} = \Phi(\sigma - \sigma_y)$ (4–6). Here σ_y is the yield stress and Φ is the cell wall extensibility. Consequently, we model the cell wall expansion following a viscoplastic analysis based on Lockhart's equation (7).

The pollen tube cell wall is treated as a thin shell of viscoplastic material (7). The pollen tube is assumed to have axial symmetry and to grow at a steady rate. The growth is assumed to be orthogonal (8), meaning that a marker particle placed on the cell wall moves in a direction normal to the cell wall during growth. The turgor pressure inside the cell creates a tensile stress in the cell wall, which as a result is deformed in a viscoplastic manner. The expansion of the cell wall is described by the following stress-strain rate relations characteristic of a viscoplastic material and previously published by Dumais et al. (2006) (7)

$$\dot{\epsilon}_i = \Phi(\sigma_e - \sigma_y)\frac{1}{|H|}\frac{\partial H}{\partial \sigma_i}, \tag{1}$$

where Φ is the extensibility, $H = \sigma_e^2/2$ the stored elastic energy and σ_e and σ_y are the effective and constant yield stresses. When eq. 1 is written explicitly in terms of s, n and θ, the strain rate components are given by

$$\dot{\epsilon}_s = \Phi(\sigma_e - \sigma_y)\Big(\frac{\sigma_s - \nu\sigma_\theta}{K}\Big), \tag{2}$$

$$\dot{\epsilon}_\theta = \Phi(\sigma_e - \sigma_y)\Big(\frac{\sigma_\theta - \nu\sigma_s}{K}\Big), \tag{3}$$

$$\dot{\epsilon}_n = \Phi(\sigma_e - \sigma_y)\Big(\frac{(\nu - 1)(\sigma_s + \sigma_\theta)}{K}\Big). \tag{4}$$

The stress components are given by

$$\sigma_s = \frac{p}{2\tau\kappa_\theta}, \tag{5}$$

$$\sigma_\theta = \frac{p}{2\tau\kappa_\theta}\Big(\frac{\kappa_s}{\kappa_\theta}\Big). \tag{6}$$

Here, κ_s and κ_θ are the cell wall curvatures along the curvilinear coordinates, τ is the cell wall thickness, and p the hydrostatic pressure. Since the tube is axysymmetric, the curvature with respect to θ can be expressed in terms of the curvature as a function of the position s along the arc of the tube. The cell wall curvature and shape are calculated in two dimensions. However, this shape contains all the information necessary to extract the 3-dimensional shape. The strain rates can be written in terms of the velocity vector component normal to tube, v_n, and component tangential to the cell wall, v_t,

$$\dot{\epsilon}_s = v_n\kappa_s + \frac{\partial v_t}{\partial s}, \tag{7}$$

$$\dot{\epsilon}_\theta = v_n\kappa_\theta + \frac{v_t\cos\varphi}{r}, \tag{8}$$

and

$$\dot{\epsilon}_n = -(\dot{\epsilon}_s + \dot{\epsilon}_\theta) + \frac{R}{\tau} = 0. \tag{9}$$

Here, R is the rate at which new material is deposited on the cell wall.

A simple algorithm for the shape of a cell growing according to the viscoplastic model can be derived in the simple case of orthogonal growth, i.e. when every point on the cell wall moves exclusively in a direction normal to the cell wall such that $v_t = 0$. One can define the strain rate anisotropy $\lambda(s) = (\dot{\epsilon_s} - \dot{\epsilon}_\theta)/(\dot{\epsilon_s} + \dot{\epsilon}_\theta)$. By substituting the equations for the strain rates into this relation, one obtains

$$\lambda(s) = \frac{(\sigma_\theta - \sigma_s)(1+\nu)}{(\sigma_\theta + \sigma_s)(1-\nu)}. \tag{10}$$

By defining the stress anisotropy $\gamma(s) = (\sigma_\theta - \sigma_s)/(\sigma_\theta + \sigma_s)$, eq. 10 yields

$$\nu = \frac{\lambda - \gamma}{\lambda + \gamma}. \tag{11}$$

Putting $v_t = 0$ in eqs. 7,8 yields $\lambda = (\kappa_\theta - \kappa_s)/(\kappa_\theta + \kappa_s)$ while substituting eqs. 5,6 into eq.11 for the stress anisotropy yields

$$\gamma = (\kappa_\theta - \kappa_s)/(3\kappa_\theta + \kappa_s). \tag{12}$$

Substituting eqs. 10,12 in terms of the principal curvatures into the eq.11, the relation

$$\kappa_s = 1 - 2\nu(\kappa_\theta) \tag{13}$$

is obtained. Since the pollen tube has axial symmetry, there is a second direct relation between the two principal curvatures. Given a function $\nu(s)$, the principal curvatures can be found be iterating the following three equations

$$\varphi(s) = \int_0^s \kappa_s^{(i)} ds, \tag{14}$$

$$\kappa_\theta^{(i)} = \frac{\sin\varphi}{r} = \sin\varphi\Big(\int_0^s \cos\varphi(s) ds\Big), \tag{15}$$

$$\kappa_s^{(i+1)} = 1 - 2\nu(\kappa_\theta^{(i)}). \tag{16}$$

During the iterations, denoted by the superscript i, the following boundary conditions must be met. At the tip, or pole, of the tube, the two principal curvatures must be equal thus $\nu(0) = 0$. At the equator of the tube, k_θ must be constant along the shank ($d\kappa_\theta/ds|_S{=}0$) and $\kappa_s = 0$. These two conditions are met by enforcing $\varphi(S) = \pi/2$ and $\nu(S) = 1/2$. Once the curvature κ_s is calculated along the arc position s, the cell wall can be reconstructed. Finally, the curvatures κ_s and κ_θ are inserted into eqs. 5 and 6 for the different stresses. Fig. 2A in the main part of the manuscript shows the shape of the cell wall during the steady viscoplastic growth that satisfy Lockhart's equation (eq. 1) and eq. 17.

Since the cell wall becomes thinner when stretched, vesicle deposition supplies the material necessary to maintain a constant thickness during the continuous elongation of the cell. The net rate R at which the vesicles fuse with the membrane (Fig. 2B in the main part of the manuscript) is assumed to be such that the thickness of the cell wall stays constant and the normal strain rate $\epsilon_n = 0$ (7). This is expressed by

$$\dot{\epsilon}_n = -\dot{\epsilon}_s - \dot{\epsilon}_\theta + \frac{R}{\tau} = 0, \tag{17}$$

where τ is the thickness of the cell wall and the ϵ_i denote the strain rates in the curvilinear coordinates. The average net fusion rate can be estimated from measured quantities (9). Multiplying the average number of vesicles per minute needed to sustain a typical growth of $7\mu m/min$ ($N_V = 3939 min^{-1}$) by the average vesicle volume ($V_{ol} = 0.0026\mu m^3$) and dividing by the total apex surface ($S_A = 415\mu m^2$) yields an average net fusion rate $R = 0.0244\mu m/min$. Furthermore, in order to achieve steady growth, the turgor pressure and the rheological parameters such as the extensibility Φ must remain constant. While the precise location of the exocytosis activity at the apex remains a subject of debate (10–13), a comparison of its average value (calculated above) with the average vesicle flux at the fringe

(see main part of the manuscript) supports the claim that the vesicle flux pattern is only marginally affected by the localisation of this activity. While we use a consistent model (eq. 17) for this process, our results do not depend on this particular model of the average vesicle secretion rate.

Actin microfilament orientation

The spatial distribution and orientation of actin microfilaments is very distinct in the shank and apical fringe of the pollen tube. Long parallel, relatively thick bundles of F-actin occur along the shank of the pollen tube (14–17)[1]. However, in the region bordering the apical cone, actin forms a dense network of less bundled filaments (16, 18–20). This region of the actin cytoskeleton is called the apical fringe. The formation and stability of the fringe as well as the filament orientation can be studied with a statistical model of actin filament aggregation (21–26). The actin filaments in the pollen tube can be classified into two distinct groups: the filaments bound to the stable array and those free to move in the cytoplasm. Free actin filaments aggregate and diffuse rotationally and translationally until they bind to the network filaments. Network filaments cannot diffuse but they aggregate and re-orient into bundles of common orientation. This can be expressed with the following reaction-diffusion model (24). We fix our coordinate system such that the tube grows toward the positive y-direction, and will model the change in orientation and density of the actin filaments along the x-direction using

$$\begin{aligned} \frac{\partial N(x,\Theta,t)}{\partial t} &= \beta_1 FK * F + \beta_2 NK * F - \gamma N, \qquad (18) \\ \frac{\partial F(x,\Theta,t)}{\partial t} &= -\beta_1 FK * N - \beta_2 FK * F + \gamma N + \mu_1 \frac{\partial^2 F}{\partial \Theta^2} + \mu_2 \frac{\partial^2 F}{\partial x^2}. \end{aligned}$$

Here $N(x,\Theta,t)$ and $F(x,\Theta,t)$ represent the network and free filaments densities. Θ is the orientation of the filaments, i.e. the angle between the filaments' barbed ends and the x-axis. β_1 and β_2 are the association rates, γ the dissociation rate and μ_1, μ_2 the rotational and translational diffusion coefficients. We use the following values in the numerical simulations $(\beta_1, \beta_2, \gamma, \mu_1, \mu_2)$=(0.5,0.5,0.1,1.0,0.5). The binding of filaments occurs at a rate that depends on relative configuration and is described by the convolu-

[1]Unless specified otherwise, all numbers refer to equations,figures or the bibliography of the Supporting material section

tion terms of the form $K * F$ (26) where

$$K * F = \int_{-\pi}^{\pi} \int_{\Omega} K(\Theta - \Theta', x - x') F(\Theta', x') d\Theta dx. \tag{19}$$

The kernel $K = K_1(x)K_2(\Theta)$ was introduced to model the re-orientation of actin filaments due to the action of cross-linking proteins (21). We use

$$K_2(\Theta) = 0.4 \quad \text{if} \quad \frac{\pi}{2} - < |\Theta - \Theta'| < \frac{\pi}{2,} \tag{20}$$

and else

$$K_2(\Theta) = 0. \tag{21}$$

The spatial dependence of the kernel is $K_1(x) = exp(-(x/20)^2)$. Our analysis is simplified by the assumption that the free filaments at the tip recently joined the network whereas the filaments in the distal region of the shank have spent a certain amount of time re-arranging and bundling. Accordingly, the state of the filament population at the tip of the apex is well represented by the solution of eqs. 19 at early times. The state of the filament population in the shank is described by the solution at late times, when $N(x, \Theta, t)$ and $F(x, \Theta, t)$ have reached their equilibrium configuration. This assumption allows us to ignore the y variable. In other words, we assume that the change in time of eqs. 19 describe the change along the y-axis of the pollen tube. The state of the filament population at the fringe is thus described by the solution of eqs. 19 at intermediate times. We set the initial distribution of network filaments to be $N(x, \Theta, t = 0) = exp(-0.1(x^2 + (\Theta + \pi/2)^2)) + exp(-0.1((x - L)^2 + (\Theta - \pi/2)^2)) + \xi$ and $F(x, \Theta, t = 0) = \xi$ where ξ is a random variable that is uniformly distributed around a positive mean. These initial conditions and the model are chosen such that the filament population at late stages adopts the configuration observed in the pollen tube shank (27). The filaments in the shank form bundles in two regions: the centre (x=0) and the cytoplasmic cortex (x=L). This is equivalent to a filament distribution presenting one density peak in the centre (x=0) and one density peak at the periphery (x=L). It is known (27) that the bundle in the centre of the shank is composed of filaments with barbed ends pointing toward the back ($\Theta = -\pi/2$), while the bundles at the periphery are composed of filaments with barbed ends pointing towards the front ($\Theta = \pi/2$).

From Fig. 1, we see that the filament density profile along the fringe is uniform, unlike it is in the shank described above. Also, the fraction of the filament population attached to the network is greater than in the apex but

smaller than in the shank. Thus, the state of the filament population in the fringe is described by the solution of eqs. 19 at a time characterised by a sudden increase in the total network filament population and by a rather uniform density profile along the x-direction (Fig. 1A). Fig. 1 shows the solution of eqs 19. From Fig. 1C, we set the time at which eqs. 19 describe the fringe to be $t_i = 10000\Delta t$. At this time, the average network filament orientation $\overline{\Theta}(x)$ along the x-direction is evaluated by $\overline{\Theta}(x) = \frac{1}{C}\int_0^L \Theta N(x, \Theta, t_i) d\Theta$ where C is a normalisation constant. The numerical solution (Fig. 1B) at $t = 10000\Delta t$ can be fitted to the linear orientation profile

$$\overline{\Theta}(x) = \frac{-\pi}{L}x - \frac{\pi}{2}. \tag{22}$$

From now on, we will drop the bar and refer to the average filament orientation along the fringe as simply $\Theta(x)$. The orientation profile could also be fitted to a sigmoid function which would yield a sharper fringe shape, as calculated in the section Profile of the actin fringe. The physical principle that allows to interpret this gradual change in filament orientation is a local elastic interaction between filaments. This elastic interaction reorients the filaments in order to minimise the local elastic stress caused by mismatched orientation between neighbouring filaments. It is thus not surprising that eq. 22 satisfies the laws of elastic polymer networks. Given the simplified case of an elastically isotropic polymer network, the stress energy is $E = \nabla^2\Theta$ (28). Eq. 22 is a solution that minimises this stress.

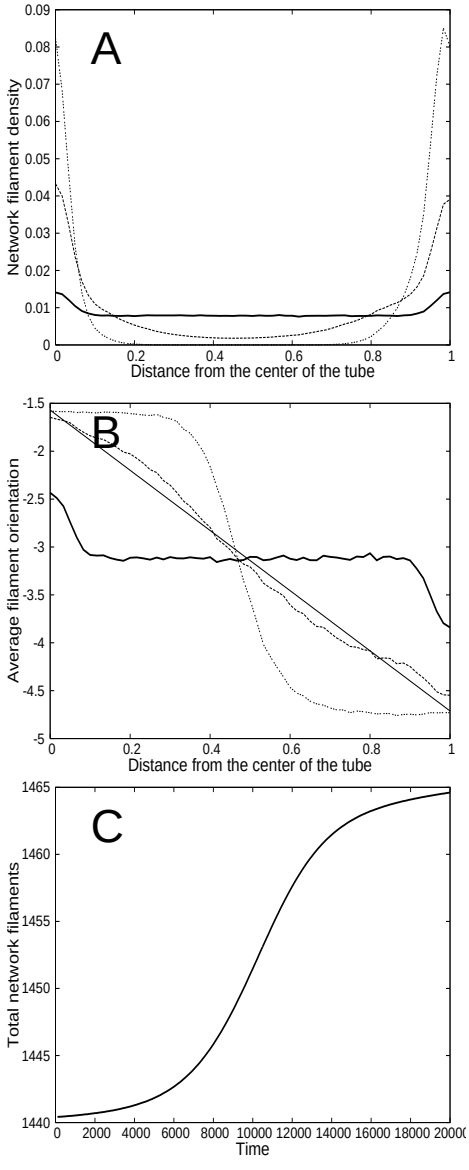

Figure 1: Dynamic aggregating and re-orientation of the actin filaments. For

Surface tension at the tail of the cone

At the tail of the apical cone, the two halves of the profile shown in Fig. 2C in the main part of the manuscript must join at a very acute angle. At that position, the curvature of the profile is very large and the surface tension γ between the actin fringe and the cytoplasm leads to capillary effects that cannot be neglected. Since the profile is parallel to the actin microfilaments, eq. 3 (in the main part of the manuscript) predicts that the normal profile velocity is zero at that location. That means that the tail of the clear zone becomes thinner and longer as the pollen tube grows, leading to an even sharper profile at its tail. The surface tension reduces the sharpness of the profile by increasing the protrusion rate as a function of the profile curvature. The pressure difference $\Delta p = \gamma K$ generated at the profile is given by the Gibbs-Thompson relation (29). Here K is the curvature given by $K = \frac{y''}{|1+y'^2|^{3/2}}$. This pressure difference acts as an effective increase in the local G-actin concentration to increase polymerisation. We approximate this effect by adding a term, valid only in regions of high curvature, to the profile velocity eq. 3 in the main part of the manuscript

$$\frac{dr}{dt} = v_{MF}\left(\mathbf{n}\cdot\mathbf{r}\right) + \frac{k_{on}\gamma K}{k_b T}, \tag{23}$$

where $k_B T$ is the energy of the thermal fluctuations. Since the microfilaments are oriented parallel to the profile at the end of the tail, the first term in the previous expression is negligible. Assuming that the end of the tail advances at the same rate v_p as the whole profile yields the equality $k_{on}\gamma K = v_p$. Expressing $K = 1/L$ where L is the radius of curvature at the end of the tail, and $k_{on} = v_{MF}/G \simeq v_p/G$, yields the chemical capillary length $L \simeq \frac{\gamma}{G k_B T}$. We estimate the order of magnitude of the capillary length to be $L \simeq 1.5\mu m$ from the width of the apical cone in Fig. 1F in the main part of the manuscript. For $G \simeq 10\mu M$ (30), the surface tension is of the order of $4 \times 10^{-5} J/m^2$. The condition that the curvature K is a constant at the end of the tail is met by a profile in the shape of a half circle

$$y = \left(L^2 - x^2\right)^{1/2}. \tag{24}$$

The contribution of the surface tension is visible at the funnel end of the actin fringe, where the two symmetric halves of the profile meet and where its curvature is maximal. The full profile is shown in the inset of Fig. 2C in the main part of the manuscript.

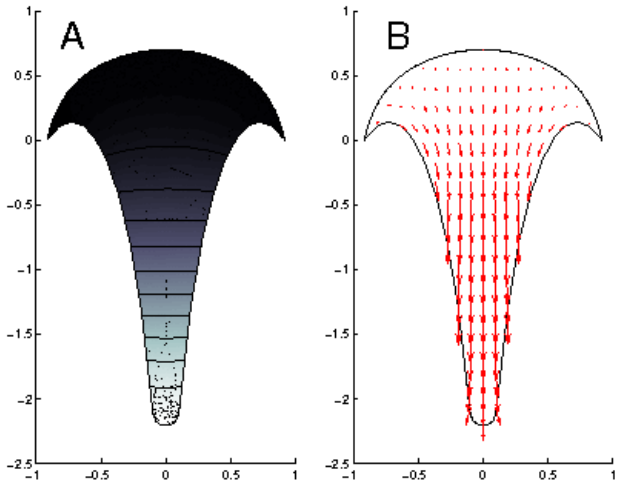

Figure 2: (A) Vesicle density in an angiosperm pollen tube without vesicle secretion. The growth rate and the parameter R are zero but the vesicle retrieval and delivery at the fringe is maintained. (B) Vesicle flux in the same pollen tube.

Effect of arrest of pollen tube growth on vesicle streaming patterns

Vidali *et al.* (14) used biochemical (profilin and DNAse) and pharmacological agents (latrunculin B and cytochalasin D) to perturb actin microfilament polymerisation and structure in growing pollen tubes. They found that these actin polymerisation inhibitors have a much stronger effect on pollen tube growth than on cytoplasmic streaming, i.e. that the concentration of inhibitor needed to stop streaming is much higher than that required to stop growth. To imitate the arrest of pollen tube growth, we set the values for R=0 for all positions along the cell wall and set the advancement and protrusion rate of the fringe to zero. The resulting vesicle movement patterns and density distribution (Fig. 2) are not significantly different from the normally growing tube (Fig. 4. in the main part of the manuscript).

Therefore, according to our model, inhibiting the polymerisation process while maintaining the acto-myosin mediated vesicle transport would not alter the vesicle flux pattern significantly as long as the shape of the clear zone remains the same. In the same way, an inhibition of vesicle secretion at the plasma membrane would not disrupt the vesicle flux pattern but only disrupt cell wall elongation and thus pollen tube growth. This behaviour was observed upon inhibition of Rho-GTPases (31). The treatment blocks vesicle exocytosis while maintaining the cytoplasmic streaming. Essentially, our model explains how the vesicle flux pattern is maintained as long as the orientation of the microfilaments and the funnel shape of the clear zone are maintained, even if the rates of actin polymerisation or pollen tube growth are affected.

Pollen culture, fluorescent label and image acquisition

This section explains the experimental methods and techniques used to obtain the pollen tube micrographs shown in Fig. 1 of the main article.

Actin label

After two hours of growth, pollen tubes were fixed for 40 seconds in 3% formaldehyde, 0.5% glutaraldehyde and 0.05% Triton X-100 solution in a buffer composed of 100 mM PIPES, 5 mM $MgSO_4$ and 0.5 mM $CaCl_2$ at pH 9. Pollen tubes were then washed 3 times for one minute each in the same buffer followed by an incubation overnight at 4^oC in rhodmine phalloidin (Molecular Probes) diluted (1:30) in a buffer composed of 100 mM PIPES, 5 mM $MgSO_4$, 0.5 mM $CaCl_2$ and 10 mM EGTA at pH 7. Subsequently, the pollen was washed 5 times for one minute each in the same buffer, mounted on glass slides in a drop of citifluor (Electron Microscopy Sciences), covered with a cover slip, sealed and immediately observed with a Zeiss Imager-Z1 microscope equipped for structured illumination microscopy (apotome) and with a Zeiss AxioCam MRm camera. A filter set of BP 546/12 excitation, FT 560 beamsplitter and BP 575-640 was used. All fixation and washing steps were conducted in a PELCO cold spot biowave 34700 at 150 Watts and 26^oC.

Vesicle label

Vesicles in living pollen tubes were labelled by adding 160 nM of the lipophilic styryl dye FM1-43 (Molecular Probes, Invitrogen) to the growth medium for five minutes. Then pollen was filtered and mounted in fresh growth medium between slide and coverslip for microscopic observations with a Zeiss LSM 510 META / LSM 5 LIVE / Axiovert 200M system. A 488 nm argon laser was used with an emission filter LP 575. Z-Stacks of 1 μm interval were

taken and image reconstruction and surface rendering were performed using AxioVision Release 4.5 software.

References

1. Benkert, R., G. Obermeyer, and F. Bentrup, 1997. The turgor pressure of growing lily pollen tubes. *Protoplasma* 198:1–8.

2. Li, Y.-Q., H.-Q. Zhang, E. Pierson, F.-Y. Huang, H. Linskens, P. Hepler, and M. Cresti, 1996. Enforced growth-rate fluctuation causes pectin ring formation in the cell wall of *Lilium longiflorum* pollen tubes. *Planta.* 200:41–49.

3. Zerzour, R., J. Kroeger, and A. Geitmann, 2009. Polar growth in pollen tubes is associated with spatially confined dynamic changes in cell mechanical properties. *Dev. Biol.* in press.

4. Lockhart, J., 1965. An analysis of irreversible plant cell elongation. *J. Theor. Biol.* 8:264–275.

5. Green, P., R. Erickson, and J. Buggy, 1971. Metabolic and physical control of cell elongation rate. *In vivo* studies in *Nitella*. *Plant Physiol.* 47:423–430.

6. Ortega, J., 1990. Governing equations for plant cell growth. *Physiol. Planta.* 79:116–121.

7. Dumais, J., S. Shaw, C. Steele, S. Long, and P. Ray, 2006. An anisotropic-viscoplastic model of plant cell morphogenesis by tip growth. *Int. J. Dev. Biol.* 50:209–222.

8. Bartnicki-Garcia, S., C. Bracker, G. Giertz, R. Lopez-Franco, and H. Lu, 2000. Mapping the growth of fungal hyphae: orthogonal cell wall expansion during tip growth and the role of turgor. *Biophys. J.* 79:2382–2390.

9. Bove, J., B. Vaillancourt, J. Kroeger, P. Hepler, P. Wiseman, and A. Geitmann, 2008. Magnitude and direction of vesicle dynamics in growing pollen tubes using spatiotemporal image correlation spectroscopy (STICS) and fluorescence recovery after photobleaching (FRAP). *Plant Physiol.* 147:1646–1658.

10. Picton, J., and M. Steer, 1983. Membrane recycling and the control of secretory activite in pollen tubes. *J. Cell Sci.* 63:303–310.

11. Derksen, J., T. Rutten, I. Lichtscheidl, A. de Win, E. Pierson, and G. Rongen, 1995. Quantitative analysis of the distribution of organelles in tobacco pollen tubes: implications for exocytosis and endocytosis. *Protoplasma* 188:267–276.

12. Moscatelli, A., F. Ciampolini, S. Rodighiero, E. Onelli, M. Cresti, N. Santo, and A. Idilli, 2007. Distinct endocytic pathways identified in tobacco pollen tubes using charged nanogold. *J. Cell Sci.* 120:3804–3819.

13. Zonia, L., and T. Munnik, 2008. Vesicle trafficking dynamics and visualization of zones of exocytosis and endocytosis in tobacco pollen tubes. *J. Exp. Bot.* 59:861–873.

14. Vidali, L., S. McKenna, and P. Hepler, 2001. Actin polymerization is essential for pollen tube growth. *Mol. Biol.Cell.* 12:2534–2545.

15. Perdue, T., and M. Parthasarathy, 1985. In situ localization of F-actin in pollen tubes. *Eur. J. Cell. Biol.* 39:13–20.

16. Lancelle, S., M. Cresti, and P. Hepler, 1987. Ultrastructure of the cytoskeleton in freeze-substituted pollen tubes of *Nicotiana alata*. *Protoplasma.* 140:141–150.

17. Lancelle, S., and P. Hepler, 1992. Ultrastructure of freeze-substituted pollen tubes of *Lilium longiflorum*. *Protoplasma* 167:215–230.

18. Heslop-Harrison, J., and Y. Heslop-Harrison, 1991. The actin cytoskeleton in unfixed pollen microwave-accelerated DMSO-permeabilisation phalloidin staining. *Sex. Plant Reprod.* 4:6–11.

19. Miller, D., S. Lancelle, and P. Hepler, 1996. Actin microfilaments do not form a dense meshwork in *Lilium longiflorum* pollen tube tip. *Protoplasma.* 195:123–132.

20. Kost, B., R. Spielhofer, and N. Chua, 1998. A GFP-mouse talin fusion protein labels plant actin filaments in vivo and visualizes the actin cytoskeleton in growing pollen tubes. *Plant J.* 16:393–401.

21. Civelekoglu, G., and L. Edelstein-Keshet, 1994. Modelling the dynamics of F-actin in the cell. *Bull. Math. Biol.* 56:587–616.

22. Alt, W., 1987. Mathematical models in actin-myosin interactions. *In* Nature and Function of Cytoskeletal Proteins in Motility and Transport., Wohlfahrt-Bottermann, K. E., editor, Gustav Fischer Verlag, Stuttgart, 219–230.

23. Mogilner, A., and E. Edelstein-Keshet, 1995. Selecting a common direction. I. How orientational order can arise from simple contact responses between interacting cells. *J. Math. Biol.* 33:619–660.

24. Mogilner, A. I., and L. Edelstein-Keshet, 1996. Spatio-angular order in populations of self-aligning objects: formation of oriented patches. *Physica D.* 89:346–367.

25. Mogilner, A., E. Edelstein-Keshet, and G. Ermentrout, 1996. Selecting a common direction. II. Peak-like solutions representing total alignment of cell clusters. *J. Math. Biol.* 34:811–842.

26. Spiros, A., and L. Edelstein-Keshet, 1998. Testing a model for the dynamics of actin structures with biological parameter values. *Bull. Math. Biol.* 60:275–305.

27. Lenartowska, M., and A. Michalska, 2008. Actin filament organization and polarity in pollen tubes revealed by myosin II subfragment 1 decoration. *Planta.* 228:891–896.

28. Chandrasekhar, S., 1992. Liquid Crystals. Cambridge University Press, Cambridge, 2nd edition edition.

29. Pelcé, P., 2000. New Visions on Form and Growth. Oxford University Press, Oxford.

30. Pollard, T., L. Blanchoin, and R. Mullins, 2000. Molecular mechanisms controlling actin filament dynamics in nonmuscle cells. *Annu. Rev. Biophys. Biomol. Struct.* 29:545–576.

31. Lin, Y., and Z. Yang, 1997. lnhibition of pollen tube elongation by microinjected anti-Ropl Ps antibodies suggests a crucial role for rho-type GTPases in the control of tip growth. *Plant Cell.* 9:1647–1659.